Hydrology and Earth System Sciences

Open Access

Discussions

Flow resistance of vegetated oblique weir-like obstacles during high water stages

S. Ali and W. S. J. Uijttewaal

Environmental Fluid Mechanics Section, Faculty of Civil Engineering and Geosciences, Delft University of Technology, P.O. Box 5048, 2600GA, Delft, the Netherlands

Correspondence to: S. Ali (s.ali@tudelft.nl)

Flow resistance of vegetated oblique weir-like obstacles

S. Ali and
W. S. J. Uijttewaal

Title Page

Abstract	Introduction
Conclusions	References
Tables	Figures

|◄ | ►|
◄ | ►

Back | Close

Full Screen / Esc

Printer-friendly Version

Interactive Discussion

Abstract

At high water stages obstacles in the flood plains of a river contribute to the flow resistance and hamper the conveyance capacity. In particular the elevated vegetated parts are expected to play an important role. The objective of this research work is to determine the form drag due to vegetated oblique weir-like obstacles. The experiments have been performed to measure the energy head losses for a range of subcritical flow conditions, varying discharges and downstream water levels. The energy head loss caused by the submerged vegetated weir-like obstacle has been modeled using an expansion loss form drag model that has been derived from one dimensional momentum conservation equation and accounts for the energy loss associated with a deceleration of the flow downstream of a sudden expansion. The results have been compared with the experimental data and showed an overall good agreement.

1 Introduction

Water level predictions for extreme events (flood waves) are very important for the design of dykes and embankments and the safety of the area behind them. During extreme discharges, the summer dikes are overflowed and a part of the river discharge flows through the winter bed with several obstacles. The winter bed contains vegetation and also weir-like obstacles such as access roads (elevated), summer embankments submerged groynes etc. These obstacles affect the flow levels during floods especially in cases with vegetation growing on top. Understanding of flow characteristics concerning summer dikes and vegetated weir-like obstacles can be helpful for river managers. These weir-like obstacles can be perpendicular or at an angle to the flow direction and can also be vegetated. The characteristics and hydraulic behavior of plain or standard weirs have been studied for a long time and the understanding on them is rather deep. However, a few studies have been done on weirs placed obliquely in the flow. The most important difference between an oblique weir and plain weir is that the crest of the

S. Ali and
W. S. J. Uijttewaal

Title Page

Abstract | Introduction

Conclusions | References

Tables | Figures

◄◄ | ►►

◄ | ►

Back | Close

Full Screen / Esc

Printer-friendly Version

Interactive Discussion

oblique weir makes an angle with the flow direction in the channel. An extreme example is the side weir, a part of the channel embankment, its crest being parallel to the flow direction in the channel (Bos, 1989). Its function is to drain water from the channel whenever the water surface rises above a predetermined level so that the channel

5　water surface downstream of the weir remains below a maximum permissible level. Aichel (1953) presented a new relation for the discharge coefficient of a round crested skewed-weir compared with the plain weir in his report (in German). Vries (1959) also did many experiments to examine the energy loss of the flow over dike-form weirs under different oblique angles and flow conditions. The main objective of his research was to

10　examine the influence of the obliqueness of the weir to the stage-discharge relation and the experiments were done on trapezoidal weirs. Borghei et al. (2003) derived a relation for the discharge coefficient for oblique rectangular sharp-crested weirs based on experimental data. Borghei et al. (2006) improved the formula for the discharge coefficient by using the incomplete self similarity (ISS) concept. Wols et al. (2006) published the

15　numerical simulations of oblique weirs using a non-hydrostatic finite elements model FINLAB, with free surface and k-ϵ turbulence closure. Tuyen (2006, 2007) measured the energy head loss and discharge coefficients under different weir configurations and flow conditions. Ali and Uijttewaal (2009, 2010) studied the vegetated weir-like structures oriented perpendicular to the flow direction and quantified the energy head loss

20　caused by such types of obstacles.

The main goal of this research is to determine the energy head loss due to the oblique vegetated weir-like structures in the floodplain and to describe the structure of the flow phenomenon related to it. We will also examine the physical processes which play a role and how the flow is influenced by such type of obstacles.

25　## 2　To determine discharge over a weir

There is an extensive knowledge on the perpendicular (plain) sharp crested weir in the literature such as Rehbock (1929), Rouse (1936), Kindsvater and Carter (1957),

Flow resistance of vegetated oblique weir-like obstacles

S. Ali and
W. S. J. Uijttewaal

Kandaswamy and Rouse (1957), Ramamurarthy et al. (1987), Swamee (1988), Hager (1984, 1993), Munson et al. (2002), Azimi and Rajaratnam (2009). Flow properties for an embankment broad crested weir has been discussed by Fritz and Hager (1998) and Sargison and Percy (2009).

Figure 1 shows the weir configurations and longitudinal section of flow over a sharp crested weir. The elementary analysis for a plain weir placed normal to the flow direction, the discharge relation in case of the perfect flow conditions is: $q_0 = \frac{2}{3} C_{df} \sqrt{\frac{2}{3} g} H_0^{\frac{3}{2}}$, where q_0 ($\mathrm{m^3\,s^{-1}\,m^{-1}}$) is the specific discharge (discharge per unit length of the weir crest), C_{df} is the discharge coefficient for perfect flow conditions, g ($\mathrm{m\,s^{-2}}$) is the gravitational acceleration and H_0 (m) is the energy head (Bos, 1989). Using energy balance on upstream side of the weir (Fig. 1), the discharge coefficient C_{df} is written as (Wols et al., 2006);

$$C_{df} = \frac{3\sqrt{3}Fr_1}{\left(2 + Fr_1^2\right)^{3/2}} \tag{1}$$

where Fr_1 ($Fr_1 = \frac{u_1}{\sqrt{gd_1}}$) is Froude No. over weir crest, d_1 (m) is the water depth and u_1 ($\mathrm{m\,s^{-1}}$) is the average velocity above the weir crest.

Depending on the downstream water depth the weir could be in a submerged or free flow condition. The general relation for the submerged specific discharge (q) of a submerged plain weir is

$$q = C_d q_0 \tag{2}$$

$$q = C_{df} C_d \frac{2}{3} \sqrt{\frac{2}{3} g} H_0^{\frac{3}{2}} = C \frac{2}{3} \sqrt{\frac{2}{3} g} H_0^{\frac{3}{2}} \tag{3}$$

where C_d is the discharge reduction coefficient and $C = C_{df} \times C_d$ is the discharge coefficient. Villemonte (1947), Govinda Rao and Muralidhar (1963), Brater and King (1976),

and Wu and Rajaratnam (1996) introduce the discharge reduction coefficient C_d for sharp crested weirs and Fritz and Hager (1998) for the embankment weir with side slopes 1 : 2 as a function of submergence $(S) = H_2/H_0$. Here H_2 (m) is the downstream energy head.

The discharge reduction coefficient (C_d) due to submergence for sharp crested weirs was given by the empirical relation of Villemonte (1947): $C_d = \left(1 - S^{1.5}\right)^{0.385}$.

The more general form for this relation which is used in practice is: $C_d = \sqrt{\left(1 - S^P\right)}$. Here P is an empirically fit parameter which is influenced by the weir geometry.

An oblique weir has a larger crest length than the channel width, which results a decrease in the specific discharge. This geometrical feature enhances the efficiency of the weir, increasing the effective weir length ($L = B/\cos\varphi$) and hence increasing the discharge for the same water head and the same channel width.

The approaches to analyze the oblique weir characteristics, found in literature are of a highly empirical nature. Aichel (1953) related the specific discharge (q_L) for an oblique weir (based on the crest length) to the specific discharge of a perpendicular weir (q) in the following way;

$$\frac{q_L}{q} = 1 - \beta_A \frac{d_0 - \Delta}{\Delta}$$

where d_0 (m) is the water depth upstream of the weir, Δ is the weir height and β_A is the coefficient depending on the angle of obliqueness. This coefficient increases with the angle of obliqueness (Fig. 2) and the specific discharge of weir decreases. Borghei et al. (2003) derived the following expression for the discharge coefficient for the perfect weir based on the experimental data.

$$C_{df} = \left(0.701 - 0.121\frac{B}{L}\right) + \left(2.229\frac{B}{L} - 1.663\right)\frac{(d_0 - \Delta)}{\Delta} \tag{4}$$

where B (m) is the width of channel and L (m) is the length of weir. For an imperfect weir the C_{df} is multiplied by a factor C_d ($C = C_{df} \times C_d$) depending on the submergence

of the weir ($\frac{d_2 - \Delta}{d_0 - \Delta}$) as follows

$$C_\mathrm{d} = \left[\left(0.008\frac{L}{B} + 0.985\right) + \left(0.161\frac{L}{B} - 0.479\right)\left(\frac{d_2 - \Delta}{d_0 - \Delta}\right)^3\right]^2 \quad (5)$$

where d_2 (m) is the water depth on the downstream side of weir. The discharge reduction coefficient (C_d) increases with the angle of obliqueness as well as the discharge. A few studies are available on oblique weirs and none on vegetated oblique weirs.

3 Mathematical formulation (analytical approach)

The theoretical analyses on weirs are important for the prediction and interpretation of experimental data. The effect of a vegetated obstacle on the flow can be considered to either induce an energy loss or exert a drag force on the flow. Yalin (1964) and Engelund (1966) assumed that the effect of bed forms on the flow is analogous to a sudden expansion in a pipe flow. The Energy loss due to a sudden pipe flow expansion is calculated using the one-dimensional (1-D) linear momentum and energy conservation equations. Karim (1999) and van der Mark (2009) considered the effects of bed form on flow as sudden expansion for the open channel flow instead of a pipe flow. Ali and Uijttewaal (2009, 2010) also studied the vegetated weir-like structures oriented perpendicular to the flow direction to quantify the energy head loss. To determine flow velocity and water depth around the weir-like structures such as a submerged groyne or a spur dike, the following assumptions can be made.

– Energy is conserved over the upstream face of the groyne or spur dike.

– Momentum is conserved over the downstream side of the groyne.

At the upstream side the streamlines are contracting and energy is conserved where as at the downstream side, there is a sudden expansion, the energy is not conserved

in this region. On the downstream side, the momentum conservation equation in longitudinal (x) direction has been applied. The continuity (the conservation of the water mass) is valid everywhere. It is assumed here that the flow is steady, frictionless and incompressible and the pressure on the weir crest is hydrostatic.

To understand the physics in a better way we use a rather straightforward approach for the energy and momentum balances as described above. For a weir inclined to the flow, the flow velocity could be decomposed into two components, parallel and perpendicular to the flume axis, it can also be decomposed into two components parallel and perpendicular to the weir axis. Theoretically it is assumed that the crest parallel component does not change its magnitude (though it has some effect), when the flow reaches the weir. The accelerating force only acts on the velocity component perpendicular to the weir crest and the same holds for the deceleration process. The angle of flow obliqueness is the deviation angle of the stream lines from the normal direction with respect to the weir crest. For the plain weir this angle is zero. For an oblique weir value of ψ can be predicted using an energy balance and the continuity requirement for the flow.

The energy balance is applied to the upstream region of the weir and it is assumed that there is no energy loss in the contraction region upstream of the weir;

$$d_0 + \frac{\alpha_0 u_0^2}{2g} = (d_1 + \Delta) + \frac{\alpha_1 u_1^2}{2g} \tag{6}$$

Here d_0, d_1, d_2 are water depths, α is the kinetic energy correction coefficient and u_0, u_1, u_2 are the depth averaged velocities at sections 0, 1, 2 respectively. The velocity is decomposed into two components, parallel and perpendicular to the weir axis such that:

$$u_0^2 = u_{0p}^2 + u_{0L}^2, \quad u_1^2 = u_{1p}^2 + u_{1L}^2 \tag{7}$$

Here subscript "p" is for perpendicular and "L" for parallel direction. The continuity equation always holds true for the flow.

$$Q = u_{0p}d_{0L} = u_{1p}d_{1L} \text{ and } q_L = u_{0p}d_0 = u_{1p}d_1 = u_{2p}d_2 \tag{8}$$

where Q is the total discharge of the flow cross-section, L (m) is the length of the oblique weir and can be calculated as $L = B/\cos\varphi$ (B is the channel width, Fig. 3). The assumption made here is that the velocity component parallel to the weir crest remains constant in the area of investigation so $u_{0L} = u_{1L}$. Using the continuity equation (Eq. 8), the energy balance (Eq. 6) can be written as;

$$d_0 + \frac{\alpha_0 u_{0P}^2}{2g} = (d_1 + \Delta) + \frac{\alpha_1 u_{1P}^2}{2g} \text{ or } d_0 + \frac{\alpha_0 q_L^2}{2gd_0^2} = (d_1 + \Delta) + \frac{\alpha_1 q_L^2}{2gd_1^2}$$

here q_L is the specific discharge, Δ is the weir height and g is the gravitational acceleration. All lengths can be non-dimensionalized by the critical water depth at the section 1. Defining the Froude number as (Chanson, 1999; Jain, 2001); $Fr_1 = \frac{u_{1p}}{\sqrt{gd_1}} = \frac{q_L}{d_1\sqrt{gd_1}}$, it gives the critical depth (d_{cr1}) above the weir crest;

$$d_{cr1} = \sqrt[3]{q_L^2/g} \tag{9}$$

This approach simplifies the equations and reveals that the dimensionless weir height Δ^* is the only parameter in the problem (Eq. 10). The dimensionless energy conservation between section 0 and 1 is written as;

$$d_0^{*3} - (d_1^* + \Delta^* + \frac{\alpha_1}{2d_1^{*2}})d_0^{*2} + \frac{\alpha_0}{2} = 0 \tag{10}$$

here * represents the dimensionless quantity. If the value of d_1^* is known, d_0^* can be found as a root of the Eq. (10).

At the downstream side there is a deceleration region. Here the energy is dissipated in the wake region. The depth averaged momentum conservation equation is applied between sections 1 and 2 as shown in Fig. 4. The expansion has been considered sudden and the pressure is assumed hydrostatic here also. Momentum conservation equation has the following form;

$$\frac{1}{2}\rho g(d_1 + \Delta)^2 - \frac{1}{2}\rho g d_2^2 = \rho q(\beta_2 u_2 - \beta_1 u_1) \tag{11}$$

here β is the momentum correction coefficient, ρ (kg m^{-3}) is the density of water. Velocity is again decomposed into two components as above in case of energy balance upstream of the weir.

$$u_2^2 = u_{2p}^2 + u_{2L}^2, \quad u_1^2 = u_{1p}^2 + u_{1L}^2 \tag{12}$$

It is assumed that the velocity component parallel to the weir crest remained constant in the area of investigation so. So Eq. (11) can be written as;

$$\frac{1}{2}\rho g(d_1 + \Delta)^2 - \frac{1}{2}\rho g d_2^2 = \rho q_L(\beta_2 u_{2p} - \beta_1 u_{1p}) \tag{13}$$

The dimensionless momentum conservation between sections 1 and 2 can be written as (van Rijn, 1990):

$$d_1^{*3} + 2\Delta^* d_1^{*2} + \left(\Delta^{*2} - d_2^{*2} - \frac{2\beta_2}{d_2^*}\right)d_1^* + 2\beta_1 = 0 \tag{14}$$

If the value of d_2^* is known, d_1^* can be found from Eq. (14). For natural channels, the correction factors (α's and β's) vary between 1.15–1.50 and 1.05–1.17 respectively. (Chow, 1959; Chaudhry, 1994).

3.1 Flow direction and oblique angle

A relation between the angle of obliqueness and the flow direction above the weir crest can be derived as given below. We have;

$$\tan\varphi = \left(\frac{u_{0p}}{u_{0L}}\right), \ \tan\psi = \left(\frac{u_{0p}}{u_{0L}}\right) \Rightarrow \frac{\tan\varphi}{\tan\psi} = \frac{u_{1p}}{u_{0p}} \tag{15}$$

The continuity equation of flow leads to $\frac{u_{1p}}{u_{0p}} = \frac{d_0}{d_1}$ and the specific discharge can be written as

$$q_{L1} = Fr_{1p}\sqrt{g}d_1^{\frac{3}{2}}, \quad q_{L0} = Fr_{0p}\sqrt{g}d_0^{\frac{3}{2}} \Rightarrow \frac{Fr_{1p}}{Fr_{0p}} = \left(\frac{d_0}{d_1}\right)^{\frac{3}{2}}, \tag{16}$$

Using Eqs. (15) and (16) the relation among ψ, φ and flow conditions reads

$$\frac{\tan\psi}{\tan\varphi} = \left(\frac{Fr_{0p}}{Fr_{1p}}\right)^{\frac{2}{3}} \tag{17}$$

The flow direction can be calculated above the weir crest using Eq. (17). As the velocity increases on the weir crest, the flow direction approaches normal to the weir crest. For free flow conditions the flow is directed almost perpendicular to the weir crest.

3.2 Weir with vegetation

3.2.1 Emerged vegetation

In this case the weir has a row of vegetation on the top of its crest and the presence of the vegetation causes extra energy losses. These vegetation elements are considered here emerged. Energy dissipation in this situation is caused by different processes. There is an interaction between the wake turbulence generated by the weir and by

the vegetation and also mutually between the wake regions of the vegetation but here these interactions have been ignored and only the depth averaged velocity distribution is considered. The effect of vegetation on the cross sectional area is considered and the depth averaged velocity is calculated in this section with reduced cross sectional area (vegetation cross sectional contraction and weir effect) (Ali and Uijttewaal, 2013). The velocities at the three cross-sections can be written as in the Eq. (18).

$$u_{0p} = \frac{q_L}{d_0} \qquad u_{1p} = \frac{q_L b}{d_1(b-D)} = \frac{q_L}{d_1}\left(\frac{1}{1-\frac{D}{b}}\right) \qquad u_{2p} = \frac{q_L}{d_2} \tag{18}$$

Here b is the centre to centre distance between two adjacent cylinders and D is the diameter of a cylinder as shown in the Fig. 5. Considering the critical flow condition above the weir crest, the critical depth of flow can be written as;

$$d_{1cr}^3\left(1 - D/b\right)^3 = \frac{q_L^2}{g}$$

The non-dimensionalized (using the critical depth) energy and momentum conservation can be written as;

$$d_0^* + \frac{\alpha_0}{2d_0^{*2}} = \Delta^* + d_1^* + \frac{\alpha_1}{2d_1^{*2}}\left(\frac{1}{1-\frac{D}{b}}\right)^2 \tag{19}$$

$$(\Delta^* + d_1^*)^2 + \frac{2\beta_1}{d_1^*}\left(\frac{1}{1-\frac{D}{b}}\right) = d_2^{*2} + \frac{2\beta_2}{d_2^*} \tag{20}$$

3.2.2 Submerged vegetation

In this case the water level exceeds the vegetation height and vegetation is submerged as shown in Fig. 5. The dimensionless energy conservation and momentum conservation between section 0 and 1 and section 1 and 2 respectively can be written as;

$$d_0^* + \frac{\alpha_0}{2d_0^{*2}} = \Delta^* + d_1^* + \frac{\alpha_1}{2d_1^{*2}} \left(\frac{1}{1 - \frac{l^*D}{d_1^*b}} \right)^2 \tag{21}$$

$$(\Delta^* + d_1^*)^2 + \frac{2\beta_1}{d_1^*} \left(\frac{1}{1 - \frac{l^*D}{d_1^*b}} \right) = d_2^{*2} + \frac{2\beta_2}{d_2^*} \tag{22}$$

Here l^* is the dimensionless vegetation length. By knowing the downstream water depth and the specific discharge, the upstream water depth and the energy head (H_0) can be determined using the analytical approach. Hence the discharge coefficient is determined as; $C = \frac{Q}{\frac{2}{3}L\sqrt{\frac{2}{3}gH_0}\frac{3}{2}}$.

3.2.3 Bed and wall resistance (to correct the experimental data)

The total energy head loss (ΔH_t) in a flume over a distance L_e can be due to the following three sources as explained by Ali and Uijttewaal (2013)

– Form drag due to obstacles (ΔH),

– Grain and skin friction of the bed (ΔH_B),

– The side wall friction (ΔH_W)

The energy losses due to the bed and wall friction can be obtained as;

$$\Delta H_{\mathrm{B}} = c_{f2} \int_0^{L_{\mathrm{e}}} \frac{u}{gd}^2 \partial \ell, \qquad \Delta H_{\mathrm{W}} = c_{f3} \int_0^{L_{\mathrm{e}}} \frac{2u}{gB}^2 \partial \ell \qquad (23)$$

where L_{e} is the length between the section 0 and 2, B is the flume width, d is water depth and u is average velocity. The friction coefficient (c_f) and friction factor (f) can be related as; $c_f = \frac{f}{8}$. The friction factor is calculated by the Colebrook-White formula (Colebrook, 1939). To compare the experimental data with the analytical results, these estimated energy losses (caused by the bed and wall friction) are deducted from the total energy head loss to get the energy loss of the vegetated weir-like obstacle.

$$\Delta H = \Delta H_{\mathrm{t}} - \Delta H_{\mathrm{B}} - \Delta H_{\mathrm{W}}. \qquad (24)$$

3.3 Model results

3.3.1 Flow direction over the weir

The Fig. 6 shows the variation of stream line angle over the oblique weir against the water depth above the weir crest and the weir height. These graphs are plotted using Eqs. (15) and (16). Figure 6a, b and c are for different weir heights. Using a constant discharge implies that the weir height is constant with respect to the critical depth. In critical flow condition (d_1^*), the water has the highest velocity and thus the most sensitive to the effect of weir. Increasing the water depth gives an imperfect weir flow condition and tends toward an unaffected flow direction for d_1 approaches to infinity especially for a low weir(e.g $\Delta^* = 0.5$). With a high weir the upstream velocity is low so the velocity above the weir is mainly due to the weir and thus almost perpendicular $\psi \to 0$.

3.3.2 Energy head loss

Figure 7a shows the variation of energy head loss against the Froude number on the weir crest for different weir heights (α and $\beta = 1$). It is seen that in all cases the energy head loss disappears when $Fr1$ goes to zero. The value of 1 is not affected by the inclination of the weir since H_0 is compared to H_2 and both are defined in the same way. At the critical flow condition ($Fr1 = 1$) the upstream water level become independent of the downstream water level.

As it is assumed that only the velocity component perpendicular to the weir is changed by the energy and momentum conservation laws, we get a weak dependence of the energy head loss on the weir inclination to the flow direction. This shows as a smaller head loss at higher inclination angles apparently because the larger inclination results in a smaller velocity component perpendicular to the weir and a subsequent smaller acceleration/deceleration cycle.

Figure 7b shows the variation of discharge coefficient against the H_2/H_0 for different weir heights. It can be expected that the discharge coefficient C will tend to one for small values of H_2/H_0. Here a problem arises with the definition of H_0. If we account for the total velocity head the discharge is overestimated since only the velocity component perpendicular to the weir contributes to the discharge. This is especially important for low weirs where the upstream velocity has a relative large contribution to H_0. Using only the perpendicular velocity component results in a curve that is not depending on the weir inclination simply because the underlying equations are identical, regardless of φ.

3.3.3 Comparison with Borghei et al. (2003)

We can make a comparison between our analytical approach and the empirical approximation by Borghei et al. (2003) as given in Sect. 2. It should be noted that for the imperfect weir case the downstream configuration of the flow domain determines the

further direction of the streamlines. The presented results therefore only hold for the specific configuration used by Borghei et al. (2003).

For the case that we consider again the perpendicular component of the velocity with respect to the weir, it could straightforwardly be treated as a standard imperfect weir. Their analysis only seems to make sense for small values of H_0/Δ in that case the height is dominant over the velocity head and $(d_0 - \Delta)/\Delta$ is approximately equal to H_0/Δ. As the definition of C_{df} is based on energy considerations a fair comparison can only be made using the right properties. Moreover for the oblique weir the definition of H_0 does not correspond to the definition of C_{df} which becomes increasingly apparent for higher values of d/Δ. For that reason it is not strange that the C_{df} value varies. The definition of C_d is a bit simpler. The graph (Fig. 8) shows the effect that a bigger inclination leads to a smaller loss.

4 Experiments

4.1 Experimental setup

The experiments were conducted in a rectangular horizontal glass flume, 19.2 m long, 2 m wide and 22 cm deep. In the middle area of the flume, an oblique weir is situated, with a height of 8 cm. To represent the floodplain roughness, the gravels of diameter 5 to 8 mm were glued on the flume bed and over the weir. The angle of obliqueness of the weir is 45°. The water for the experiments was taken from and returned to the main circulation system in the laboratory. The flow from a 250 mm conduit was discharged into a stilling basin and then into the experimental flume. Discharge of water to the flume was measured by an electromagnetic flow meter mounted on the conduit (Fig. 9).

For the study a prototype trapezoidal dike of height 6 m with a crest width 3 m and the side slopes 1V : 4H (both, upstream and downstream side) is used. The model is made of composite, wood and concrete material. The side slopes of the model weir were 1V : 4H (same like a prototype). The oblique model weir has a height of 8 cm

(crest width 4 cm, scale 1/75) because of the flume depth limitations, with the upstream and downstream slopes of 1 : 4. The vegetation on the weir crest was modeled by the circular cylinders. The relative vegetation blockage on the weir crest was 25 %. The height of the model plants is 4 cm and the diameter is 1.2 cm (Fig. 10).

4.2 Measuring equipments

4.2.1 Point gauges

Point gauges are used to measure the flow depth for energy loss and discharge calculations. These are also used to draw the free surface profile. To measure the water depths first the elevation of the water surface and then the elevation of the bed at that point was measured. To get the value of flow depth, the later was subtracted from the first. There were two point gauges mounted on a moveable beam in such a way that the measurement can be made across the flume. The beam itself is mounted on the flume on two side rails. Point gauges were used to measure the height of the free surface and the bed level to an accuracy of ±0.1 mm.

With supercritical flows, the water surface is highly unstable behind the weir due to undulations and hydraulic jumps and sometimes there was air entrainment. These aspects together decreased the accuracy of water level determination to ±1 mm. Far down stream, the flow surface calmed down and the accuracy of the depth measurement can be considered as normal (±0.1 mm).

4.2.2 Laser displacement Sensors

Laser displacement sensors (ILD1300) are used to measure the water depth 2 m (from centre of the weir) upstream and 3 m down stream of the weir. It is an optical sensor for measurements with micrometer accuracy. These sensors use the principle of optical triangulation, i.e. a visible, modulated point of light is projected onto the target surface. Depending on the distance the diffuse fraction of the reflection of this point of light is

then focused onto a position sensitive element (CCD-array) the controller calculates the measured value from the CCD-array. An internal close-loop control enables the sensor to measure against different surfaces. The laser beam is directed perpendicular onto the surface of the target. Point gauge is used to measure the water depth on the crest of the weir with an accuracy of ±0.1 mm.

4.2.3 Acoustic Doppler Velocimeter (ADV)

The Acoustic Doppler Velocimeter (ADV) was used to measure the (3-Dimensional velocity components) velocity profiles at different locations around the vegetated weir.

It is a 3-D velocity sensor which transmits acoustic pulses into water. These pulses are then scattered by the particles present in water. The echo is received as with LDA, by the receivers of the ADV and the Doppler shift is calculated from the segments of the echo. The echo is Doppler shifted in proportion to the particle velocity.

4.3 Experimental programme

4.3.1 Energy head loss measurements

Tests have been carried out (for an oblique weir) for several flow conditions by varying the discharge and down stream water level. The inflow has been provided with the discharge of 20, 25, 30, 35, 40 L s^{-1}. For each discharge the down stream water depth was adjusted and gradually varied to give the 15 different flow states, from completely sub-merged to the free flow regime. After adjustment, almost 10 min are required to stabilize the flow and then the water depth and velocity measurements can be performed. The Different cases for an oblique weir with a down stream slope of 1 : 4 are

- model Weir with out vegetation,

- model Weir with cylinders (25 % blockage area).

For these measurements the dimensionless weir height (Δ^*) varies from 4 to 8.

4.3.2 Velocity measurements

The velocity measurements were taken via an acoustic Doppler Velocimeter (ADV) at selected discharges of 25 and $30\,\mathrm{L\,s}^{-1}$. At one cross section approximately 10 velocity points have been measured with decreasing distance between them form top to bottom.
5 These velocity measurements will be used for latter flow analysis.

5 Result and discussion

5.1 Non-Vegetated oblique weir

The measured data can be used to calculate some dependent flow parameters. The most important one is the discharge coefficient (C) as defined in Eq. (3). It represents
10 the flow rate over the weir and reflects the losses caused by the weir. The relative upstream water head (H_0/Δ) provides a better view for a general situation. Its relation with the discharge coefficient is shown in Fig. 11a.

Discharge coefficients have been extracted from the measured data using the Eq. (3) in Sect. 2. With a certain discharge, C decreases as the relative upstream water head
15 increases. In the same figure, the right graph shows the variation of discharge coefficient with the Froude number ($Fr1$) on the weir crest and a comparison with the analytical results (Eq. 1). When the Froude number is low (high submergence flow condition), the loss in water head from upstream to down stream section is also small. By decreasing the down stream water level gradually the flow turned to undulating and
20 then emerged, and the energy losses increased as well.

In Fig. 12 discharge reduction coefficient (C_d) is plotted against the submergence for the inclination angle 45°. The discharge reduction coefficient based on the oblique weir length and based on the channel width (B) is plotted and it is also plotted for the plain weir. This figure also presents the discharge reduction coefficient deduced from

Flow resistance of vegetated oblique weir-like obstacles

S. Ali and
W. S. J. Uijttewaal

Title Page

Abstract | Introduction

Conclusions | References

Tables | Figures

|◄ | ►|

◄ | ►

Back | Close

Full Screen / Esc

Printer-friendly Version

Interactive Discussion

the Villemonte (1947) relationship using different p values. The graph based on Eq. (5) (Borgei's relation) has been drawn in this figure as well.

This figure clearly depicts that the results for Borghei et al. (2003) have a significant variation from the experimental data. The relationship given by Borghei et al. (2003) is a highly empirical and also very much dependent on the experimental conditions. The experimental data which have been applied to derive the formula (Borghei et al., 2003) are mainly taken form the experiments which are performed for a rectangular sharp-crested weir. It means that this relation is only applicable for sharp crested weirs, whereas the present weir is of a trapezoidal type weir with upstream and downstream slopes (1 : 4). The reason for the deviation can be the difference in experimental conditions, the weir type and the empiricism of the formula.

It can be seen from this figure that if the discharge coefficient is calculated based on the weir length, it is the same as for the plain weir. On the other hand if this is calculated based on the channel width, its value increases by a factor L/B (1.414 in case of oblique angle $\varphi = 45°$) times the C_d for a plain weir.

5.2 Comparison of energy head loss and discharge coefficient predicted by the expansion loss form drag model with experimental data for non-vegetated oblique weirs

Figure 13 shows the comparison between analytical and experimental data for the discharge coefficient. The results are plotted for the different inclinations of 0, 45 and 60°. The analytical results are calculated for dimensionless weir heights (Δ^*) 4, 6 and 8. The Discharge coefficient is plotted versus the submergence (H_2/H_0). The experimental data for the angle of inclination 0 and 60° has been taken from Vries (1959) and Tuyen (2006) for dyke form weirs (upstream and downstream slopes are 1 : 4). For small downstream water levels, the flow condition over the weir crest becomes critical and results in constant discharge coefficients. It is also clear from the figure that C increases with increasing the inclination due to the increased length of the weir crest which is

given as: $L = B\cos\varphi$. The discharge capacity could be twice for $\varphi = 60°$ as compare to the perpendicular weir.

This limiting value is not obtained here, as the part of kinetic energy on the upstream side of the weir (due to the parallel velocity component) does not contribute to the discharge. Despite of the fact that the overall agreement between the analytical results and the experimental results is quite well, these results show that the expansion loss form drag model can be applied to the oblique weir-like obstacles considering velocity decomposition as explained in Sect. 3.

Figure 14 shows the comparison of the discharge coefficients which are predicted by the expansion loss form drag model and the experimental data for the different angles of inclination. For the low angle of inclination the predicted results are more accurate. Obviously the results are more deviating for the high obliqueness. It is due to the effect of the velocity component which is ignored and also the strong deflection of flow and the complex flow structure in the wake of the weir.

The mean relative error in the predictions for the obliqueness angle 0, 45 and 60° is 4, 7 and 11 % respectively. It shows that as the angle of inclination increases the error in the results become higher because the ignored velocity component parallel to the weir crest attains higher value.

Figures 13 and 14 depicts significant deviation of predicted discharge coefficient at higher values (submergence lower then 0.8 and $Fr \geq 0.6$). As the water depth on the weir crest decreases, (Froude number on the weir crest increases) the stream lines are curved and the non-hydrostatic pressure plays a significant role but the assumption for the expansion loss form drag model remains hydrostatic.

5.3 Velocity direction on the crest of oblique weirs

It is assumed in the theoretical analysis that the weir-like obstacle does not affect the parallel velocity component (parallel to the weir crest). As the measurements by Tuyen (2006) show that the velocity components perpendicular and the parallel to the weir crest are uniform along the weir length and only show some deviation near the side

walls. On the downstream side of the weir, the deflected flow interacts with the sidewalls and this uniformity is gradually lost and the deflected flow in some case even gives rise to the horizontal flow separation. The parallel velocity component is constant except in the near wall region and at the downstream side of the weir. The above mentioned assumption for the parallel component is valid for the regions which are away from the walls. The flow tends to change angle closer to the direction perpendicular to the weir crest when flow depth decreases.

Figure 15 shows the comparison of the analytically computed flow direction (Eq. 17) at the weir crest with measured data (Tuyen, 2006). The results are showing satisfactory agreement between measured and predicted values. Analytical results for flow directions are based on energy conservation at the upstream side of the weir and continuity equation of the flow. The mean relative error for the predicted velocity direction on the weir crest in both cases is 15 %. The analytically predicted results are somewhat smaller than the expected ones. The experimental results are based on the surface velocities from PTV analyses instead of the average velocities, so this can be the reason for deviation of data from the theory.

5.4 Comparison of the energy head loss caused by the vegetated and non-vegetated oblique weirs

Figure 16 presents the comparison of the energy head loss of vegetated and non-vegetated weirs for different discharges. It also shows the theoretically predicted results using the expansion loss form drag model discussed in Sect. 3 for vegetated and non-vegetated oblique weirs. It is clear from the figure that the energy head loss increased due to the extra blockage (vegetation blockage) on the weir crest. Pseudo vegetation on weir crest also enhances the turbulence in the flow which increases the energy head loss. As can be seen from the measurement data the influences of some main hydraulic parameters to the energy head loss can be summarized as follow:

- With the same discharges, the head loss decreases with the increase of the downstream water head (increase the submergence).

- With the same down stream water depth, the higher the discharge the bigger the head loss.

- At the free flow state, the relationship between downstream water depth and the energy head loss is linear.

- The extra blockage (25 %) due to pseudo vegetation has significantly enhanced the energy head loss.

5.5 Comparison of energy head loss predicted by the expansion loss form drag model with experimental data for Vegetated oblique weirs

The expansion loss form drag model which is developed in Sect. 3 for the vegetated weir has been used to predict the energy head loss caused by the vegetated weir-like obstacles. The weir and vegetation on its crest contract the flow path in vertical and horizontal direction followed by a sudden expansion causing a deceleration region behind the weir. Energy head loss is caused due to this expansion region, having a flow separation region. The expansion loss form drag model is based on the assumption that the velocity component parallel to the weir crest remains constant, is applied to get the energy head loss caused by the vegetated oblique weir. The vegetation is considered as a horizontal contraction of the flow cross-section. In case of submerged vegetation, the shear layer between slow and fast moving water in and above the vegetation also contribute to the energy loss. To include this effect the energy and momentum correction factors (α, β) are used. α and β values which are used here are 1.18 and 1.03 respectively (Ali and Uijttewaal, 2010). Figure 17 shows the comparison of energy head loss for the vegetated weir between the predicted results by the expansion loss form drag model and the experimental data.

The results predicted by this simple model have an approximate mean relative error of 22 %. There is a deviation for the measured results in case of low energy head loss which could be attributed to the inaccuracy of measurement. In case of vegetated oblique weirs the results are under predicted. In this simple theoretical model we ignored the velocity component parallel to the oblique weir but this component does sense the vegetated elements on the weir crest, that could explain why the model under-estimates the energy head loss here. For higher energy head loss the deviation from the predicted results is due to the surface curvature and the non-hydrostatic pressure starts to contributes typically for Froude number higher than 0.6 (Ali and Uijttewaal, 2013).

6 Conclusions

Vegetated weir-like obstacles in the floodplain are important features when it is related to determine the flood flow capacity and water levels in order to design safe embankments. With a fairly simple expansion loss form drag model which is based on principle of energy and momentum conservation, quite accurate results related to the energy head loss and the flow direction over the weir crest can be obtained.

It is found that vegetation on the crest of the weir give rise to a substantial increase in energy head loss. Some main conclusions could be drawn from this study;

Changing the downstream water level will lead to changes in the flow regime and the behavior of the flow over the oblique weir. With low down stream water level, there is usually a classical hydraulic jump. Increasing the downstream water level further, the hydraulic jump will change into an undular jump.

– The energy dissipation has its maximum value for the case of a hydraulic jump behind weir, and minimum value for the case of completely submerged flow.

– Flow always turns its direction when it reaches and passes the weir, towards an almost perpendicular orientation with respect to crest.

- For perfect weir flow conditions the flow is directed almost perpendicular to the weir crest but for high water levels flow is less affected and keeps its direction.

- The discharge of an oblique weir is much higher than the discharge of a perpendicular weir with the same channel width because of the higher effective length and a hardly smaller discharge coefficient.

- The velocity decomposition proves to be an important step in studying the flow over an oblique weir without vegetation. The velocity component perpendicular to the weir accounts for most of the change in the total velocity, whereas the parallel component stays almost unchanged.

- The higher angle of obliqueness causes more error in the predicted results as the ignored parallel velocity component becomes larger.

- The energy head loss increased due to the extra blockage (vegetation blockage) on the weir crest. Pseudo vegetation on the weir crest also enhances the turbulence in the flow which increases the energy head loss.

- The expansion loss form drag model can be used to predict the discharge coefficient and energy head loss caused by the oblique vegetated obstacles. It is only applicable to submerged flow conditions where the hydrostatic pressure assumption is valid. It gives better results for low angle of obliqueness and low Froude numbers.

Title Page

Abstract | Introduction

Conclusions | References

Tables | Figures

◄ | ►

◄ | ►

Back | Close

Full Screen / Esc

Printer-friendly Version

Interactive Discussion

References

Aichel, O. G.: Abflusszahlen fur schiefe weher, (Discharge ratios for oblique weirs), Z.VDI, 95, 26–27, 1953. 5493, 5495

Ali, S. and Uijttewaal, W. S. J.: Form drag due to vegetated weir-like obstacles interpreted as expansion loss, 33rd IAHR world congress Vancouver Canada, 139–146, 2009. 5493, 5496

Ali, S. and Uijttewaal, W. S. J.: Flow resistance of vegetated weir-like obstacles during high water stages, Proceedings of river flow, Braunschweig Germany, 293–299, 2010. 5493, 5496, 5512

Ali, S. and Uijttewaal, W. S. J.: Flow resistance of vegetated weir-like obstacles during high water stages, J. Hydraul. Eng., 139, 325–330, 2013. 5501, 5502, 5513

Azimi, A. H. and Rajaratnam, N.: Discharge characteristics of weirs of finite crest length, J. Hydraul. Eng., 135, 1081–1085, 2009. 5494

Brater, E. F. and King, H. W.: Handbook of hydraulics, 6th Edn., McGraw-Hill, New York, 1976. 5494

Borghei, S. M., Vatannia, Z., Ghodsian, M., and Jalili, M. R.: Oblique rectangular sharp-crested weir, Water Mar. Eng., 156, 185–191, 2003. 5493, 5495, 5504, 5505, 5509

Borghei, S. M., Kabiri-Samani, A. R., and Nekoee, N.: Oblique weir equation using incomplete self- similarity, Can. J. Civil Eng., CSCE, 33, 1241–1250, 2006. 5493

Bos, M. G.: Discharge measurement structures, 3rd edn. ILRI, Wageningen, the Netherlands, 1989. 5493, 5494

Chanson, H.: The Hydraulics of open channel flow, Willey, New York, 1999. 5498

Chaudhry, M. H.: Open Channel flow. Prentice-Hall International, 1994. 5499

Chow, V. T.: Open channel hydraulics, McGraw-Hill, Tokyo, 1959. 5499

Colebrook, C. F.: Turbulent flow in pipes with particular reference to the transition region between the smooth and rough pipe laws, J. Inst. Civ. Eng. Lond., 11, 133–156, 1939. 5503

Engelund, F.: Hydraulic resistance of alluvial streams, J. Hydraul. Eng. Div., 92 (HY2), 315–326, 1966. 5496

Fritz, H. M. and Hager, W. H.: Hydraulics of Embankment Weirs, J. Hydraul. Eng., 124, 963–971, 1998. 5494, 5495

Govida Rao, N. S. and Muralidhar, D.: Discharge characteristics of Weirs of finite crest length, La Houille Blanche, 5, 537–545, 1963. 5494
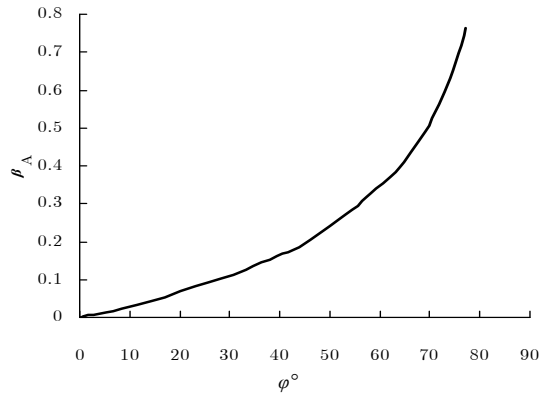
Hager, W.H.: Breitkroniger Überfall, Wasser, Energie, Luft, 1993 (in German). 5494

Flow resistance of vegetated oblique weir-like obstacles

S. Ali and
W. S. J. Uijttewaal

Title Page

Abstract | Introduction

Conclusions | References

Tables | Figures

◄ | ►

◄ | ►

Back | Close

Full Screen / Esc

Printer-friendly Version

Interactive Discussion

Hager, W. H.: Die Verlustbeiwerte in Rohren und Gerinnen, Wasser ,energie, luft-eau, Energie, air 76 Jahrgang, Heft 11/12 ,CH-5401 Baden, 253–261, 1993 (in German). 5494

Jain, S. C.: Open channel flow, John Wiley and Sons, New York, 2001. 5498

Kandaswamy, P. K. and Rouse, H.: Characteristics of flow over terminal weirs and sills, J. Hydraul. Div ASCE, 83, 1–13, 1957. 5494

Karim, F.: Bed-form geometry in sand bed-flows, J. Hydraul. Eng., 125, 1253–1261, 1999. 5496

Kindsvater, C. E. and Carter, R. W. C.: Discharge Characteristics of Rectangular Thin-Plate Weirs, Journal of the Hydraulics Division, Proc. Am. So. Civil Eng., 83, HY6, Paper 1453, 1957. 5493

Munson, B. R., Young, D. F., and Okiishi, T. H.: Fundamentals of fluid mechanics, 4th Edn., John Wiley & Sons, Inc, 2002. 5494

Ramamurarthy, A. S., Tim, U. S., and Rao, M. J.: Flow over sharp crested plate weirs, J. Irrig. Drain. Eng., 113, 163–172, 1987. 5494

Rehbock, T.: Discussion of precise weir measurements, Trans., ASCE, 93, 1143–1162, 1929. 5493

Rouse, H.: Discharge characteristics of the free overfall, Civil Eng., ASCE 6, 257–260, 1936 . 5493

Sargison, J. E. and Percy, A.: Hydraulics of board-crested weirs with varying side slopes, J. Irrig. Drain. Eng. ASCE, Jan/February 2009, 115–118, 2009. 5494

Swamee, P. K.: Generalized Rectangular Weir equations, J. Hydraul. Eng., ASCE, 14, 945–949, 1988. 5494

Tuyen, N. B.: Flow over oblique weirs, MSc, Thesis, TU Delft, 2006. 5493, 5509, 5510, 5511

Tuyen, N. B.: Influences of the oblique Obstacles to the flow, Japan-Vietnam Estuary Workshop, 2007. 5493

van der Mark, C. F.: A Semi-Analytical Model for form drag of river bed forms, Ph.D. thesis, University of Twente, the Netherlands, 2009. 5496

van Rijn. L. C.: Principles of fluid flow and surface waves in rivers, estuaries, seas and oceans, Aqua Publications, the Netherlands, 1990. 5499

Villemonte, J. R.: Submerged Weir Discharge Studies, Eng. News Record, 193, 866–869, 1947. 5494, 5495, 5509

Vries, M. De.: Scheef aangestrooomde overlaten, Rapport model onderzoek WL-Delft Hydraulics, 1959. 5493, 5509

Flow resistance of vegetated oblique weir-like obstacles

S. Ali and
W. S. J. Uijttewaal

Title Page

Abstract | Introduction

Conclusions | References

Tables | Figures

|◄ | ►|

◄ | ►

Back | Close

Full Screen / Esc

Printer-friendly Version

Interactive Discussion

Wols, B. A, Uijttewaal, W. S. J., Labeur, R. J., and Stelling, G.: Rapidly varying flow over oblique weirs, Proceedings of the 7th Int.Conf. On Hydroscience and Engineering (ICHE-2006), September 13, Philadelphia, USA, 1–13, 2006. 5493, 5494

Wu, S. and Rajaratnam, N.: Submerged flow regimes of rectangular sharp-crested weirs, J. Hydraul. Eng., ASCE, 122, 412–414, 1996. 5495

Yalin, M. S.: On the average velocity of flow over a mobile bed, La Houille Blanche, 1, 45–53, 1964. 5496

(a). Top view of a plain weir

(b). Top view of an oblique weir

(c). Side view of a sharp crested weir
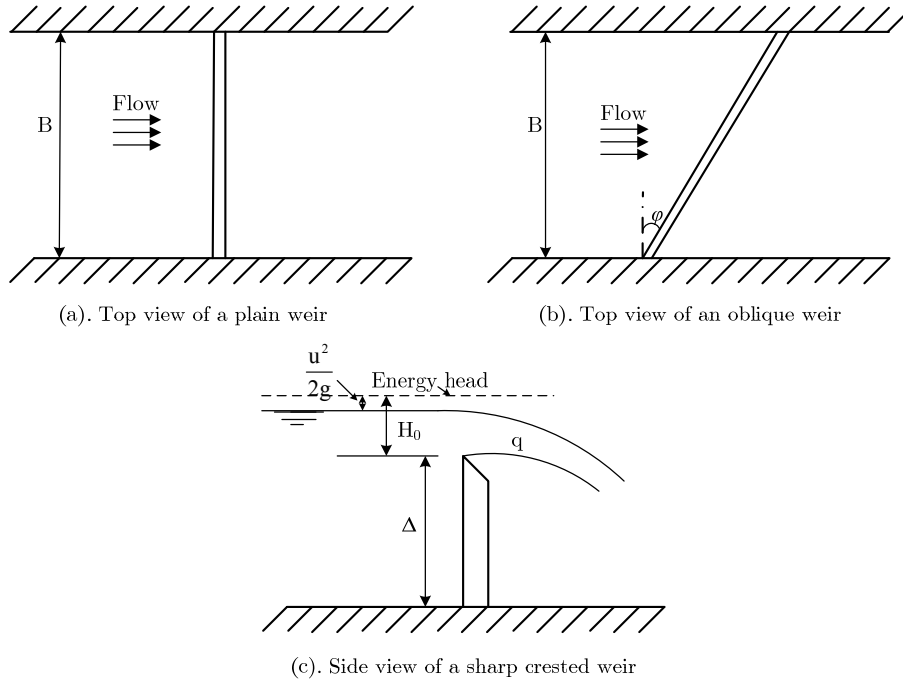
Fig. 1. Plane and side views of the weirs.

Fig. 2. β_A-values as a function of the angle of obliqueness ($\varphi°$) (Bos, 1989).
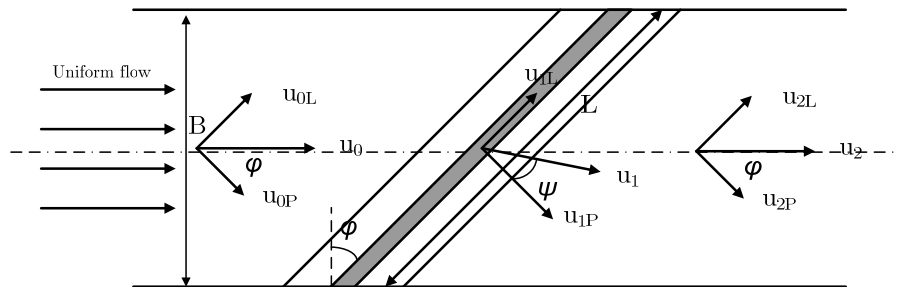
Fig. 3. Velocity decomposition upstream, at the crest and downstream of an oblique weir.

$$\frac{q^2}{2gd_0^2}$$

0

$$\frac{q^2}{2gd_1^2}$$

1

Energy head line

$$\frac{q^2}{2gd_2^2}$$

2

H_0

d_0

Flow

H_2

d_1

d_2

Model weir

Δ

1:4

1:4

Gravel
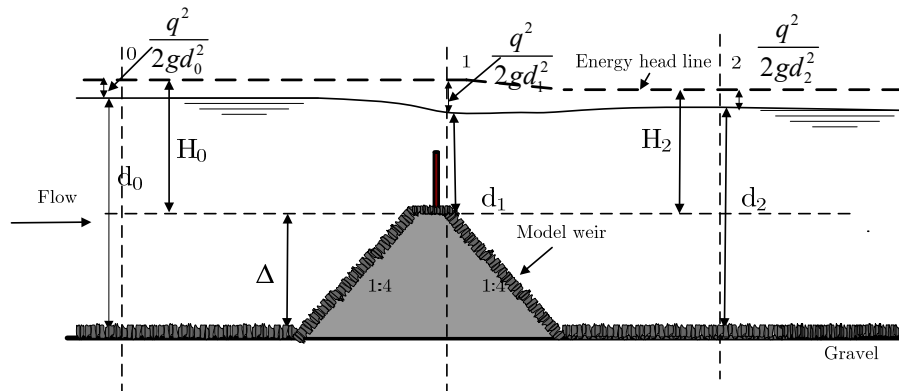
Fig. 4. Side-view of the vegetated oblique weir and flow over the weir with rough surfaces.
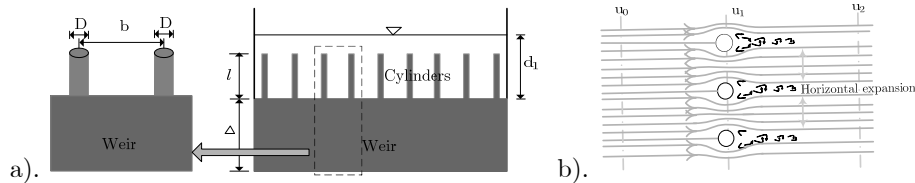
Fig. 5. (a) Cross section of vegetated weir at Sect. 1, **(b)** Flow around the pseudo vegetation on the weir crest (Top view).
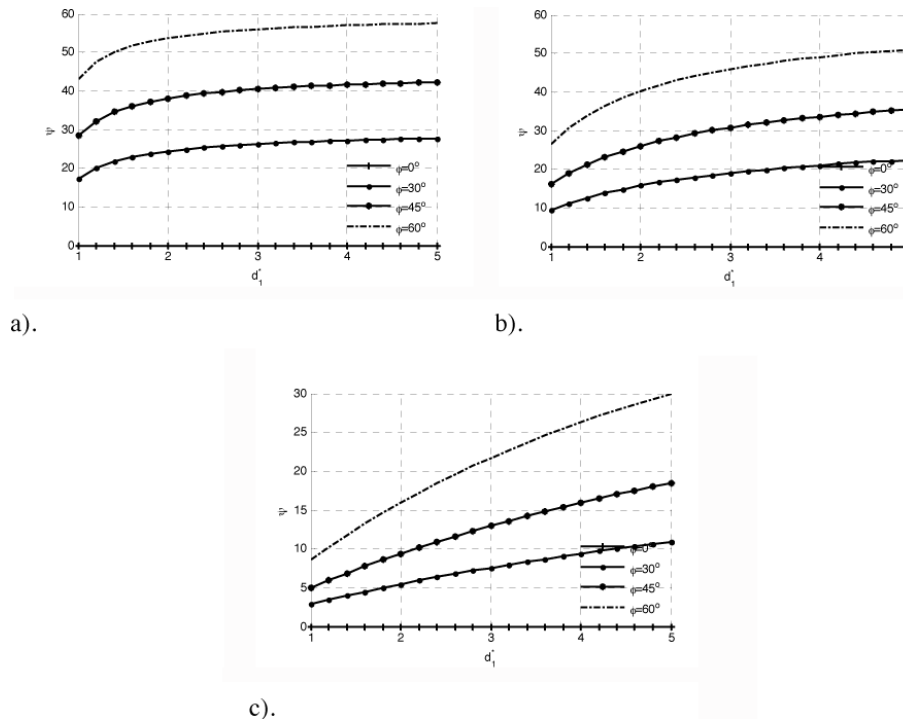
Fig. 6. Flow direction on the weir crest versus water level on the weir crest **(a)**. $\Delta^* = 0.5$, **(b)**. $\Delta^* = 2$, **(c)**. $\Delta^* = 10$.

a).

b).
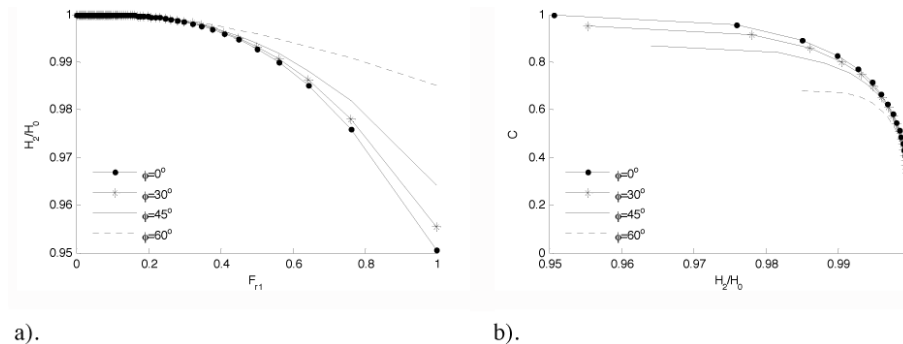
Fig. 7. Variation of energy head loss against the Froude no. on the weir-crest **(a)**, Variation of discharge coefficient against the energy head loss **(b)**, for $\Delta^* = 0.5$.

a).   b).
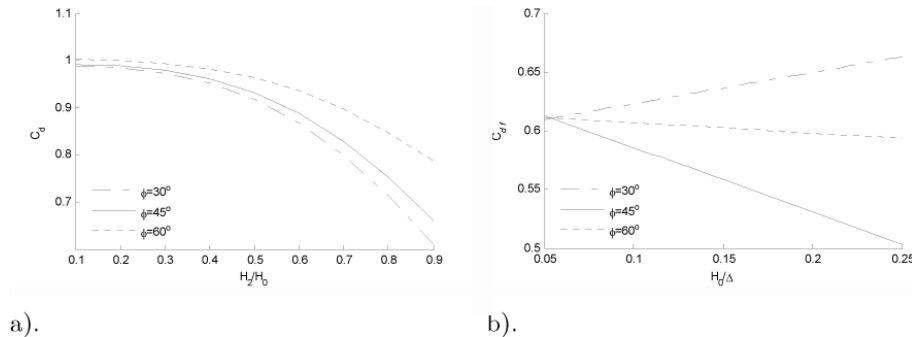
Fig. 8. Discharge coefficient variation according to Borghei et al. (2003), **(a)** discharge reduction coefficient for imperfect weir (C_d), **(b)** and free flow discharge coefficient (C_{df})
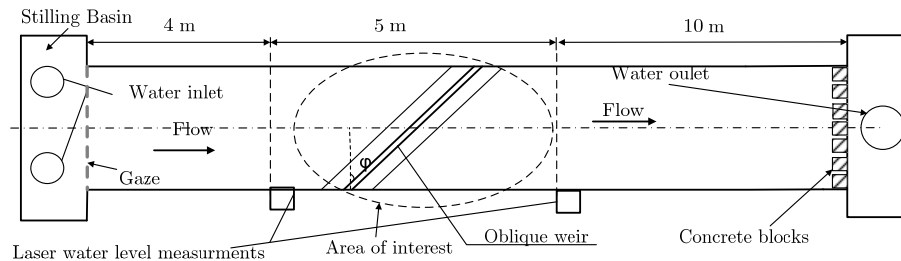
Fig. 9. Schematized plane view of the flume and measuring apparatus.

Fig. 10. Prototype dyke and model weir (scaled 1 : 75)

Title Page

Abstract | Introduction

Conclusions | References

Tables | Figures

Back | Close

Full Screen / Esc

Printer-friendly Version

Interactive Discussion
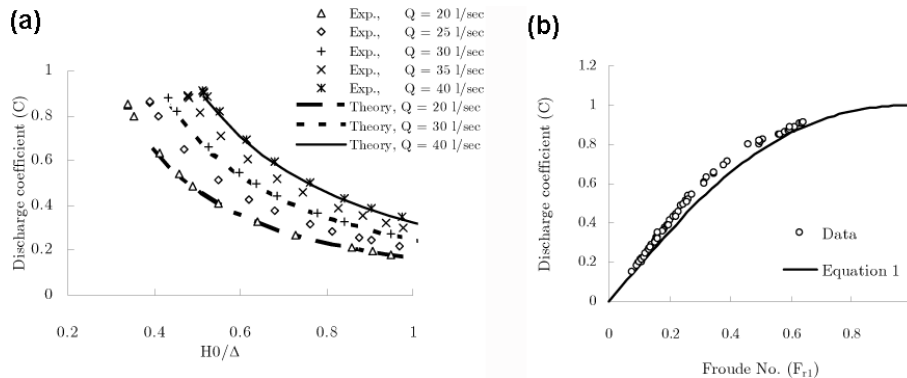
Fig. 11. Discharge coefficient (C) variation versus upstream energy head (non-dimensioned by weir height, **(a)**), Discharge coefficient variation versus Froude no. on weir crest **(b)**.
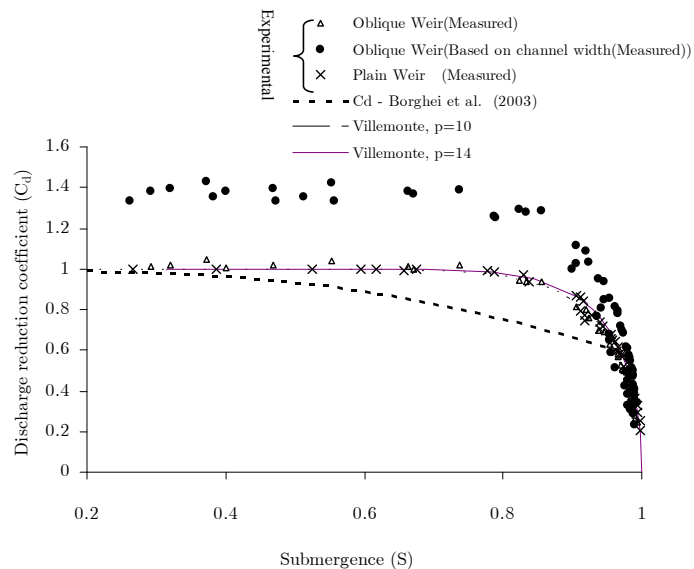
Fig. 12. Discharge reduction coefficient (C_d) versus submergence, S (angle of obliqueness is 45°).

Full Screen / Esc
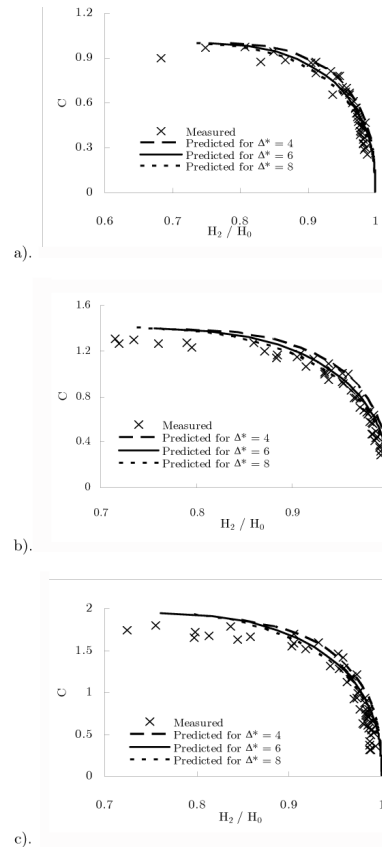
Fig. 13. Discharge coefficients (Based on channel width($B = L * \cos\varphi$)) for different angles of obliqueness, measured and predicted data is compared for different downstream water levels, Inclination angle 0° **(a)**, 45° **(b)**, 60° **(c)**.
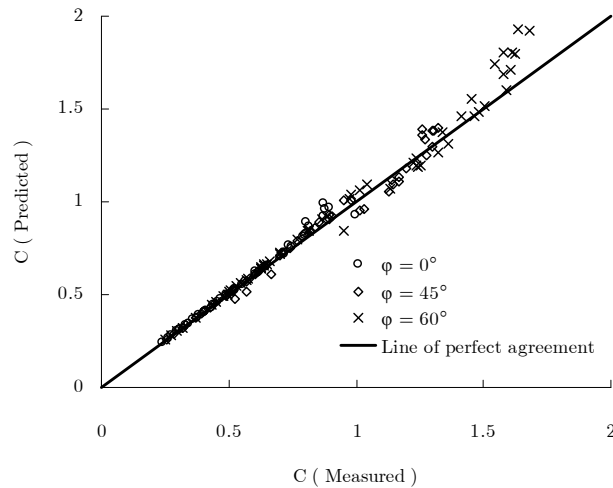
Fig. 14. Comparison of predicted and measured discharge coefficients (based on channel width $B = L * \cos\varphi$).
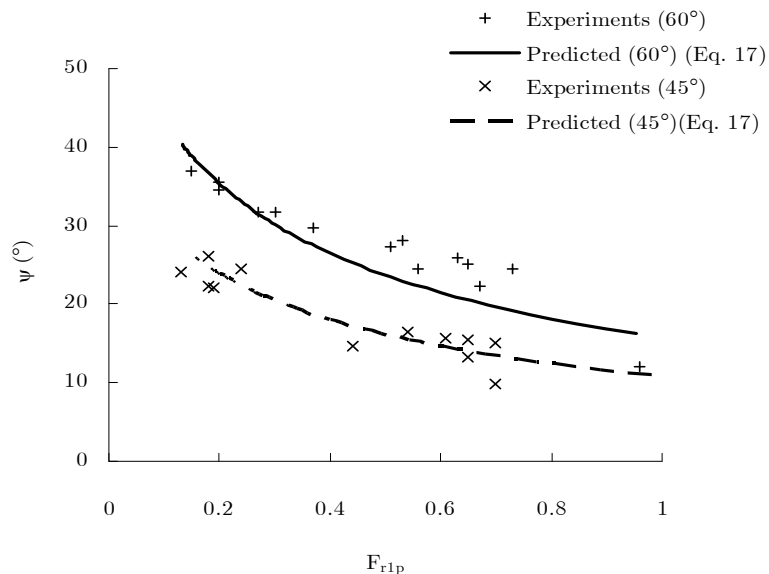
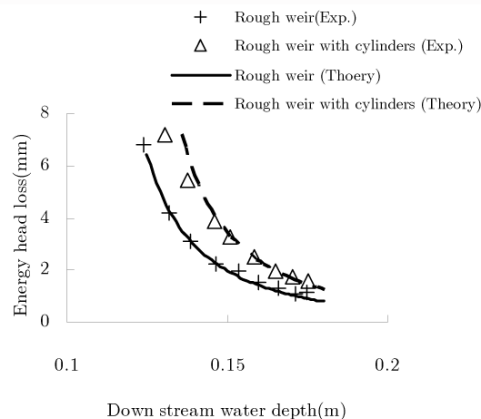**Fig. 15.** Flow direction on the weir crest versus Froude no. at the weir crest for oblique weirs.

a).
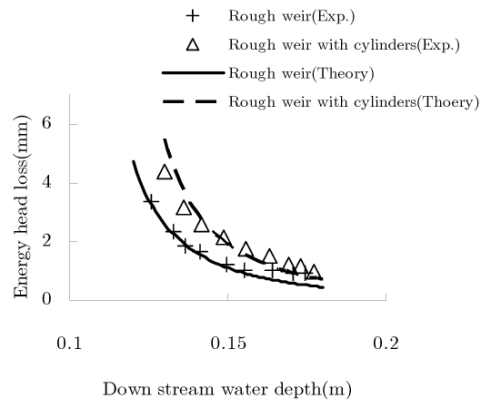
b).

Fig. 16. Comparison of energy head loss for vegetated (submerged vegetation) and non-vegetated oblique weir (Oblique angle, 45°), $Q = 40\,\mathrm{L\,s^{-1}}$. **(a)**, $Q = 30\,\mathrm{L\,s^{-1}}$ **(b)**.
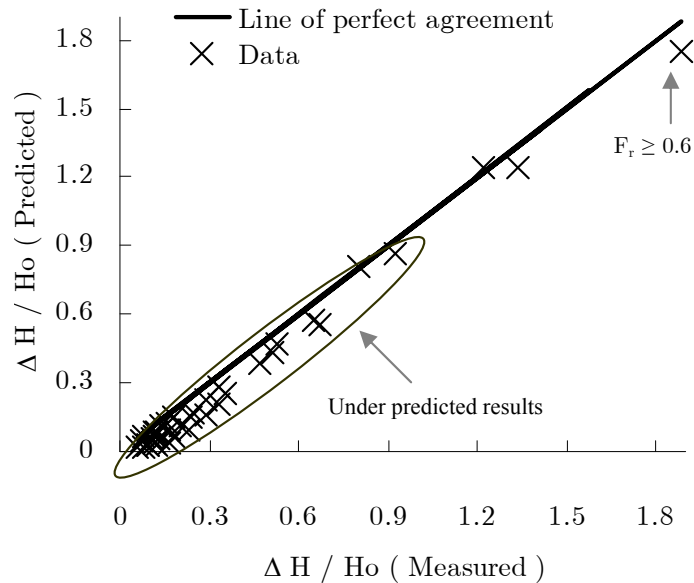
Fig. 17. Comparison of energy head loss (For a weir with vegetation, angle of obliqueness is 45˚), $\alpha = 1.18$ and $\beta = 1.03$.